IEEE Access
Multidisciplinary | Rapid Review | Open Access Journal

Received September 16, 2019, accepted October 1, 2019, date of publication November 4, 2019,
date of current version November 18, 2019.

Digital Object Identifier 10.1109/ACCESS.2019.2951504

Influence of Two-Stage Coupled Arm Inductors on Modular Multilevel Converter

KE SHEN[1,2], (Member, IEEE), SHAOZHE WANG[3], (Student Member, IEEE), DAN ZHAO[1], (Student Member, IEEE), AND GUODONG ZHAO[1], (Student Member, IEEE)

[1]School of Automation, Northwestern Polytechnical University, Xi'an 710072, China
[2]Shaanxi Key Laboratory of Small & Special Electrical Machine and Drive Technology, Xi'an 710072, China
[3]Department of Electrical and Computer Engineering, Texas A&M University, College Station, TX 77843, USA

Corresponding author: Ke Shen (kshen@nwpu.edu.cn)

This work was supported in part by the Fundamental Research Funds for the Central Universities under Grant 3102019ZDHKY10, and in part by the National Natural Science Foundation of China under Grant 51507142.

ABSTRACT The arm inductors of a modular multilevel converter (MMC) system are the necessity for the operation of the system, and the two kinds of arm inductors exist: separated inductor and coupled inductor (CI). The impact of series connection CIs on the MMC has not been fully explored. This paper provides an accurate estimation of the circulating currents of the CIs based MMC with a variety of two-stage configurations by using the combinations of positive- and negative-coupled inductors. In addition to this, a decoupling equivalent method is developed and equivalent circuits of each CI configuration are proposed. The influences of two-stage CIs on the harmonic components in circulating currents are discussed with emphasis on the even-order harmonic through the proposed estimation methodology. Simulation results are presented to demonstrate the effectiveness and accuracy of the proposed estimation as well as decoupling equivalent method. Finally, the correctness of theoretical analysis is validated with experiments.

INDEX TERMS Modular multilevel converter, arm inductor, two-stage coupled inductor, decoupling equivalent method, circulating current.

I. INTRODUCTION

As a new generation of DC transmission technology, the high voltage DC transmission (HVDC) has recently undergone rapid growth on the global scale [1]–[4]. The thyristor-based line-commutated converter (LCC) technology for HVDC gets mature with the years, but the flaws of the LCC [5]–[7], such as commutation failure, low-frequency harmonics, and the need for a large amount of reactive power compensation devices, limit its applications and performance. Recently, thanks to the development of power electronic technology, the emergence of fully-controlled power semiconductor devices such as GTO and IGBT contributes to a trend that voltage source converter based HVDC (VSC-HVDC) has become increasingly popular in the industry [1], [8], [9].

Due to the inherent modular structure, the modular multilevel converters (MMCs) offer several prominent advantages including modularity, expansibility and high waveform quality [10]–[12], so MMC has continuously absorbed much of attention and since it was introduced [13]–[17]. However, there are also some drawbacks of MMCs including circulating currents, which are harmful to the performance of the MMC and even affect the stable operation of it [18], [19]. Therefore, the circulating current suppression is one of the key technologies for MMCs, and a large number of relative studies have been conducted recently [20]–[24].

According to [25], even if a DC power source is used instead of a capacitor in SMs, the circulating currents still exist. Consequently, in addition to advance SM capacitor voltage control strategy, designing a new MMC topology based on the quantitative relationship between the circulating current and circuit parameters is another way to suppress the circulating currents. Compared with separated inductors, CIs have the advantages of small size, relatively fast transient response and high saturation current. The efforts that tried to introduce CIs into MMC have been addressed by a number of researches. References [26], [27] demonstrates a new topology of MMC with CIs is able to increase the

The associate editor coordinating the review of this manuscript and approving it for publication was B. Chitti Babu.

number of output voltage levels. A novel coupled arm inductor for MMC is proposed in [28], [29], which is compared with the standard non-coupled inductor and the center-tapped inductor and claims a significant saving of inductor material. Reference [30] proposes a set of three three-legged, six-winding ''zigzag'' inductors, which compared with the three-phase, three-winding inductors, reduces 40% size and weight. A more comprehensive study of this kind of inductor is presented in [31]. A new circuit topology of MMC that replaces arm inductors with transformers, owning a similar characteristic as CI, is discussed in [32] to diminish the voltage rating of capacitors and the power semiconductor devices by one half. The effect of the coupled arm inductor on the transient response, the capacitor voltage ripple, the circulating current, the DC short-circuit current and the switch power losses of the MMC has been examined in [33]. However, these discussions about MMC with CIs focus only on the negative-coupled inductor (NCI). They do not involve the effect of the positive-coupled inductor (PCI) on the circulating current, nor do they involve the effect of the combination of PCIs or NCIs those connected in series on circulating currents.

The contribution and objective of this paper is to analyze the influence of two-stage CIs on circulating currents of the MMC through deduced even-order harmonic expressions.

The paper is structured in the following way. Section II provides the fundamental concepts of MMC, defines parameters in the MMC system and derives the even-order harmonic expression of the circulating current based on the MMC operation principle. Section III introduces the CI and discusses the internal electromagnetic relationship. At the same time, the two-stage CI topologies that connect in series are presented and analyzed according to decoupling equivalent method. The MMCs with different kinds of CI under different power and different power factor are simulated through MATLAB/Simulink in section IV to valid the correctness of even-order harmonic expression as well as decoupling equivalent method. Section V shows the experimental results. A conclusion is stated in the Section VI.

II. MMC OPERATION PRINCIPLE AND CIRCULATING CURRENT ANALYSIS

A. OPERATION PRINCIPLE

Fig. 1 shows the basic structure of a three-phase modular multilevel power conversion system. The basic unit of the MMC is the submodule (SM) that consists of two fully-controlled power electronic switching devices Q_1, Q_2 two freewheeling diodes and a capacitor, as shown in Fig. 1, where U_{SM} represents the output voltage of a SM, i_{SM} represents the input current for this SM. Through the action of Q_1 and Q_2, U_{SM} can switches between capacitor voltage V_C and 0 in two current directions.

An entire three-phase MMC system consists of six arms, each of which consists of N interconnected and identically constructed SMs, an equivalent resistance R, and an arm inductor L. The equivalent resistance R is used to produce

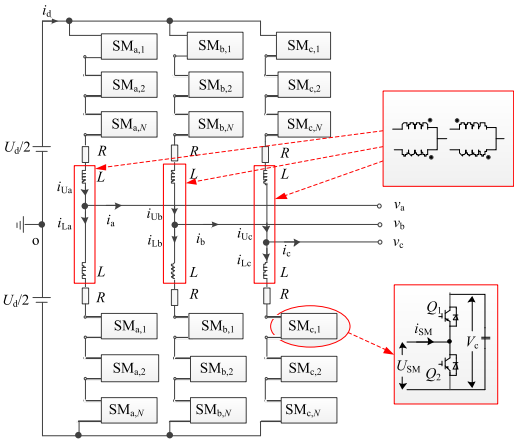

FIGURE 1. Topology of the three-phase MMC with CIs.

the equivalent MMC arm loss, inductor L plays a role in suppressing high-frequency circulating currents and providing DC side short-circuit protection. The separate inductors could be replaced by CIs as shown in Fig. 1, and the details about CIs will be discussed in Section III. One pair of upper and lower arms of MMC is viewed as one phase, and the three phases are exactly symmetrical.

When the MMC operates in steady state, the number of SMs put into the circuit one phase is N, and the DC voltage is evenly distributed to N SMs. Therefore, by adjusting the number of SMs in the on state of the upper and lower arms, the three-phase AC voltage output will be altered.

B. ANALYSIS OF THE CIRCULATING CURRENTS

The three-phase of MMC is parallel connected on the DC side, and the equivalent circuit is shown in Fig. 2. Since the upper and lower arms are combined together, the resistance and inductance of the equivalent circuit are two times compared with that of a single arm, and the two DC voltage sources are transformed into one source as well. In Fig. 2, i_{Za} represents the circulating current of phase a, i_{Zb} represents the circulating current of phase b and i_{Zc} represents the circulating current of phase c. Δu_a represents the voltage of all SMs in phase a, Δu_b and Δu_c represent the voltage of all SMs in phase b and c respectively, and the nth-order voltage harmonic of all SMs, take phase a as an instance, is denoted as Δu_a^n.

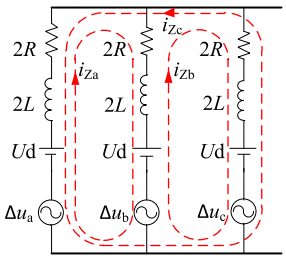

FIGURE 2. Equivalent circuit of the MMC.

The states (on or off) of each SM at specific times affect the voltage of all SMs, leading MMC to output a sinusoidal voltage. As the instantaneous energy of the MMC is stored in the capacitors of the SMs, there is an imbalance in the energy distribution between each SM as well as each phase, which directly contributes to the existence of the circulating current in MMC.

The accurate estimation of the circulating current extends the derivation in [16]. The deductive process begin with arm current, it is indicated as (1) in phase a.

$$\begin{cases} i_{\mathrm{Ua}}(t) = \dfrac{\sqrt{2}}{2} I_{\mathrm{a}} \sin(\omega t + \varphi) + I_{\mathrm{ad}} + I_2 \sin(2\omega t + \theta) \\ i_{\mathrm{La}}(t) = -\dfrac{\sqrt{2}}{2} I_{\mathrm{a}} \sin(\omega t + \varphi) + I_{\mathrm{ad}} + I_2 \sin(2\omega t + \theta) \end{cases} \tag{1}$$

In (1), I_{a} represents the RMS value of the fundamental component in the AC side output current, and φ represents the corresponding phase angle. In the following discussion, although the emphasis will be placed on harmonic amplitude analysis, the phase angle will be still useful in later calculations. I_{ad} represents the DC component of the arm current, I_2 represents the magnitude of the second-order harmonic of the circulating current, and θ represents its phase angle.

Reference [13] proves the existence of circulating currents and points out that the second-order harmonic is the main component, but the existence of other high-order harmonics will also affect the operation of the MMC to a certain extent. So, it is necessary to correct (1) to a more accurate circulating current expression by introducing the fourth-order harmonic component. The amplitude and phase angle of the fourth-order harmonic is represented by I_4 and ξ respectively, then (1) can be transformed to (2).

$$\begin{cases} i_{\mathrm{Ua}}(t) = \dfrac{\sqrt{2}}{2} I_{\mathrm{a}} \sin(\omega t + \varphi) + I_{\mathrm{ad}} + I_2 \sin(2\omega t + \theta) \\ \qquad\qquad + I_4 \sin(4\omega t + \xi) \\ i_{\mathrm{La}}(t) = -\dfrac{\sqrt{2}}{2} I_{\mathrm{a}} \sin(\omega t + \varphi) + I_{\mathrm{ad}} + I_2 \sin(2\omega t + \theta) \\ \qquad\qquad + I_4 \sin(4\omega t + \xi) \end{cases} \tag{2}$$

During the MMC operation process, all of the SMs in one phase are treated as a whole, so it is convenient for calculation to adopt a switching function. Take phase a as an example, the switching function can be written as follow,

$$\begin{cases} \sum_{k=1}^{N} S_{\mathrm{Ua\_}k}(t) = \dfrac{N}{2} - S_{\mathrm{a}} \\ \sum_{k=1}^{N} S_{\mathrm{La\_}k}(t) = \dfrac{N}{2} + S_{\mathrm{a}} \end{cases} \tag{3}$$

In (3), $S_{\mathrm{Ua\_}k}$ represents the switching function of the kth SM that located in the upper arm, and $S_{\mathrm{La\_}k}$ represents the switching function of the kth SM that located in the lower arm. S_{a} represents the switching function of the phase a terminal, and can be expressed according to the Fourier expansion,

$$S_{\mathrm{a}}(t) = \frac{N}{2} m \sin(\omega t) + \sum_{n=2}^{\infty} A_n \sin(n\omega t + \theta_n) \tag{4}$$

where m represents the modulation index, n represents the order of harmonics in the switching function of the phase a terminal. When the number of SMs N is large enough or the switching frequency is high enough, the harmonic part in (4) is very small and can be omitted. Therefore, in the case of high-frequency or multi-SM, the average switching function for each SM is shown in (5).

$$\begin{cases} \overline{S_{\mathrm{Ua}}}(t) = \dfrac{1}{2} - \dfrac{1}{2} m \sin(\omega t) \\ \overline{S_{\mathrm{La}}}(t) = \dfrac{1}{2} + \dfrac{1}{2} m \sin(\omega t) \end{cases} \tag{5}$$

In (5), $\overline{S_{\mathrm{Ua}}}(t)$ and $\overline{S_{\mathrm{La}}}(t)$ respectively represent the upper arm and the lower arm average switching function of SMs. In the following analysis, (5) will be used as switching function for each SMs.

When MMC operates in steady state, the current flowing through any SM is expressed as,

$$\begin{cases} i_{\mathrm{Ua}}(t) = \overline{S_{\mathrm{Ua}}}(t) i(t) \\ i_{\mathrm{La}}(t) = \overline{S_{\mathrm{La}}}(t) i(t) \end{cases} \tag{6}$$

In (6), i represents the current that flow through arms, i_{Ua} and i_{La} indicate the current passing through capacitors of upper and lower arm SMs respectively. Substitute $\overline{S_{\mathrm{Ua}}}(t)$ and $\overline{S_{\mathrm{La}}}(t)$ with the switching function shown in (5), the current passing through the capacitor of each SM is transformed as (7).

$$\begin{cases} i_{\mathrm{Ua}}(t) = \left[\dfrac{1}{2} - \dfrac{1}{2} m \sin(\omega t)\right] \times i_{\mathrm{Ua}}(t) \\ i_{\mathrm{La}}(t) = \left[\dfrac{1}{2} + \dfrac{1}{2} m \sin(\omega t)\right] \times i_{\mathrm{La}}(t) \end{cases} \tag{7}$$

With the extension of (7), (8), as shown at the bottom of the next page, will be obtained, which shows each component of the circulating current in detail.

The nth-order harmonic of SM voltage can be deduced by multiplying nth-order harmonic of current and capacitor reactance. By multiplying $1/(j\omega C)$, $1/(j2\omega C)$, $1/(j3\omega C)$, $1/(j4\omega C)$ and $1/(j5\omega C)$, first-, second-, third-, fourth- and fifth-order harmonic of SM voltage can be deduced as shown in (9), (10), (11), (12), (13).

$$\begin{cases} \Delta u_{\mathrm{Uc1}}(t) = \dfrac{m I_{\mathrm{ad}}}{2\omega C} \cos(\omega t) - \dfrac{\sqrt{2} I_{\mathrm{a}}}{4\omega C} \cos(\omega t + \varphi) \\ \qquad\qquad - \dfrac{m I_2}{4\omega C} \sin(\omega t + \theta) \\ \Delta u_{\mathrm{Lc1}}(t) = -\dfrac{m I_{\mathrm{ad}}}{2\omega C} \cos(\omega t) + \dfrac{\sqrt{2} I_{\mathrm{a}}}{4\omega C} \cos(\omega t + \varphi) \\ \qquad\qquad + \dfrac{m I_2}{4\omega C} \sin(\omega t + \theta) \end{cases} \tag{9}$$

$$\begin{cases} \Delta u_{\mathrm{Uc2}}(t) = \dfrac{\sqrt{2}mI_{\mathrm{a}}}{16\omega C}\sin(2\omega t+\varphi) \\ \qquad\qquad -\dfrac{I_2}{4\omega C}\cos(2\omega t+\theta) \\ \Delta u_{\mathrm{Lc2}}(t) = \dfrac{\sqrt{2}mI_{\mathrm{a}}}{16\omega C}\sin(2\omega t+\varphi) \\ \qquad\qquad -\dfrac{I_2}{4\omega C}\cos(2\omega t+\theta) \end{cases} \tag{10}$$

$$\begin{cases} \Delta u_{\mathrm{Uc3}}(t) = \dfrac{mI_2}{12\omega C}\sin(3\omega t+\theta) \\ \qquad\qquad -\dfrac{mI_4}{12\omega C}\sin(3\omega t+\xi) \\ \Delta u_{\mathrm{Lc3}}(t) = -\dfrac{mI_2}{12\omega C}\sin(3\omega t+\theta) \\ \qquad\qquad +\dfrac{mI_4}{12\omega C}\sin(3\omega t+\xi) \end{cases} \tag{11}$$

$$\begin{cases} \Delta u_{\mathrm{Uc4}}(t) = -\dfrac{I_4}{8\omega C}\cos(4\omega t+\xi) \\ \Delta u_{\mathrm{Lc4}}(t) = -\dfrac{I_4}{8\omega C}\cos(4\omega t+\xi) \end{cases} \tag{12}$$

$$\begin{cases} \Delta u_{\mathrm{Uc5}}(t) = \dfrac{mI_4}{20\omega C}\sin(5\omega t+\xi) \\ \Delta u_{\mathrm{Lc5}}(t) = -\dfrac{mI_4}{20\omega C}\sin(5\omega t+\xi) \end{cases} \tag{13}$$

The AC side output voltage is obtained through the multiplication of average switching function and SM voltage, which is displayed in (14).

$$\begin{cases} \Delta u_{\mathrm{Uo}}(t) = [\Delta u_{\mathrm{Uc1}}(t)+\Delta u_{\mathrm{Uc2}}(t)+\Delta u_{\mathrm{Uc3}}(t)+\Delta u_{\mathrm{Uc4}}(t) \\ \qquad\qquad +\ \Delta u_{\mathrm{Uc5}}(t)]\times\left[\dfrac{1}{2}-\dfrac{1}{2}m\sin(\omega t)\right] \\ \Delta u_{\mathrm{Lo}}(t) = [\Delta u_{\mathrm{Uc1}}(t)+\Delta u_{\mathrm{Uc2}}(t)+\Delta u_{\mathrm{Uc3}}(t)+\Delta u_{\mathrm{Uc4}}(t) \\ \qquad\qquad +\Delta u_{\mathrm{Uc5}}(t)]\times\left[\dfrac{1}{2}+\dfrac{1}{2}m\sin(\omega t)\right] \end{cases} \tag{14}$$

The sum of each SM output voltage is expressed as (15),

$$\begin{aligned} \Delta u(t) &= N\Delta u_{\mathrm{Uo}}(t)+N\Delta u_{\mathrm{Lo}}(t) \\ &= \Delta u_1(t)+\Delta u_2(t)+\Delta u_3(t)+\Delta u_4(t)+\Delta u_5(t) \end{aligned} \tag{15}$$

The subscript 1, 2, 3, 4, 5 represent the first-, second-, third-, fourth- and fifth-order harmonic of the sum of each SM's output voltage respectively. By expanding (15), the detailed function about the sum of each SM's output voltage can be derived as (16), as shown at the bottom of this page.

Since second-order and fourth-order harmonic are the main focus, only these two components are taken into consideration in the following discussion, and the second-order harmonic is shown in (17), as shown at the bottom of this page.

It should be noted that there are two unknown quantities, second-order and fourth-order harmonic of the output voltage in (17). Since the magnitude of the fourth-order harmonic is relatively smaller than that of the second-order harmonic, the

$$\begin{cases} i_{\mathrm{Ua}}(t) = \dfrac{1}{2}I_{\mathrm{ad}}-\dfrac{\sqrt{2}}{8}mI_{\mathrm{a}}\cos\varphi-\dfrac{1}{2}mI_{\mathrm{ad}}\cos\varphi+\dfrac{\sqrt{2}}{4}I_{\mathrm{a}}\sin(\omega t+\varphi)-\dfrac{1}{4}mI_2\cos(\omega t+\theta)+\dfrac{\sqrt{2}}{8}mI_{\mathrm{a}}\cos(2\omega t+\xi) \\ \qquad +\dfrac{1}{2}I_2\sin(2\omega t+\theta)+\dfrac{1}{4}mI_2\cos(3\omega t+\theta)-\dfrac{1}{4}mI_4\cos(3\omega t+\xi)+\dfrac{1}{2}I_4\sin(4\omega t+\xi)+\dfrac{1}{4}mI_4\cos(5\omega t+\xi) \\ i_{\mathrm{La}}(t) = \dfrac{1}{2}I_{\mathrm{ad}}-\dfrac{\sqrt{2}}{8}mI_{\mathrm{a}}\cos\varphi+\dfrac{1}{2}mI_{\mathrm{ad}}\cos\varphi-\dfrac{\sqrt{2}}{4}I_{\mathrm{a}}\sin(\omega t+\varphi)+\dfrac{1}{4}mI_2\cos(\omega t+\theta)+\dfrac{\sqrt{2}}{8}mI_{\mathrm{a}}\cos(2\omega t+\xi) \\ \qquad +\dfrac{1}{2}I_2\sin(2\omega t+\theta)-\dfrac{1}{4}mI_2\cos(3\omega t+\theta)+\dfrac{1}{4}mI_4\cos(3\omega t+\xi)+\dfrac{1}{2}I_4\sin(4\omega t+\xi)-\dfrac{1}{4}mI_4\cos(5\omega t+\xi) \end{cases} \tag{8}$$

$$\begin{aligned} \Delta u(t) = &-\frac{\sqrt{2}mNI_{\mathrm{a}}}{8\omega C}\sin\varphi+\frac{m^2NI_2}{8\omega C}\cos\theta-\frac{m^2NI_{\mathrm{ad}}}{4\omega C}\sin(2\omega t)+\frac{\sqrt{2}mNI_{\mathrm{a}}}{8\omega C}\sin(2\omega t+\varphi) \\ &-\frac{m^2NI_2}{8\omega C}\cos(2\omega t+\theta)+\frac{\sqrt{2}mNI_{\mathrm{a}}}{16\omega C}\sin(2\omega t+\varphi)-\frac{NI_2}{4\omega C}\cos(2\omega t+\theta)-\frac{m^2NI_2}{24\omega C}\cos(2\omega t+\theta) \\ &+\frac{m^2NI_4}{24\omega C}\cos(2\omega t+\xi)+\frac{m^2NI_2}{24\omega C}\cos(4\omega t+\theta)-\frac{NI_4}{8\omega C}\cos(4\omega t+\xi)-\frac{m^2NI_4}{24\omega C}\cos(4\omega t+\xi) \\ &-\frac{m^2I_4}{40\omega C}\cos(4\omega t+\xi)+\frac{m^2NI_4}{40\omega C}\cos(6\omega t+\xi) \end{aligned} \tag{16}$$

$$\Delta u_2(t) = -\frac{m^2NI_{\mathrm{ad}}}{4\omega C}\sin(2\omega t)+\frac{3\sqrt{2}mNI_{\mathrm{a}}}{16\omega C}\sin(2\omega t+\varphi)-\frac{NI_2}{4\omega C}\cos(2\omega t+\theta)-\frac{m^2NI_2}{6\omega C}\cos(2\omega t+\theta)+\frac{m^2NI_4}{48\omega C}\cos(2\omega t+\xi) \tag{17}$$

$$\Delta u_{2e}(t) = -\frac{m^2NI_{\mathrm{ad}}}{4\omega C}\sin(2\omega t)+\frac{3\sqrt{2}mNI_{\mathrm{a}}}{16\omega C}\sin(2\omega t+\varphi)-\frac{NI_2}{4\omega C}\cos(2\omega t+\theta)-\frac{m^2NI_2}{6\omega C}\cos(2\omega t+\theta) \tag{18}$$

last item in (17) is ignored in order to calculate the value of the second-order harmonic, and (17) is approximated as (18), as shown at the bottom of the previous page, which used as the expression of second-order harmonic in SMs' output voltage in the following part.

Equation (19) indicates the expression of fourth-order harmonic in SMs' output voltage.

According to the equivalent circuit of MMC, each harmonic of circulating currents equals to the corresponding harmonic of SM output voltage in one phase divided by the reactance of arm inductor as shown in (20).

$$\Delta u_4(t) = -\frac{NI_4}{16\omega C}\cos(4\omega t+\xi) + \frac{m^2NI_2}{48\omega C}\cos(4\omega t+\theta) - \frac{m^2NI_4}{30\omega C}\cos(4\omega t+\xi) \tag{19}$$

$$\begin{cases} I_2\sin(2\omega t+\theta) = -\dfrac{\Delta u_2(t)}{j2\omega 2L} \\ I_4\sin(4\omega t+\xi) = -\dfrac{\Delta u_4(t)}{j4\omega 2L} \end{cases} \tag{20}$$

Substitute (18) and (19) into (20), the expressions of the second-order and fourth-order harmonics in the circulating current are shown in (21).

$$\begin{cases} I_2 = \dfrac{\sqrt{(A\cos\varphi+B)^2+(A\sin\varphi)^2}}{1-\frac{N}{16\omega^2CL}-\frac{m^2N}{24\omega^2CL}} \\ A = \dfrac{3\sqrt{2}mNI_a}{64\omega^2CL}, \quad B = -\dfrac{m^2NI_{ad}}{16\omega^2CL} \\ I_4 = \dfrac{\frac{m^2NI_2}{192\omega^2CL}}{-1+\frac{N}{64\omega^2CL}+\frac{m^2N}{120\omega^2CL}} \end{cases} \tag{21}$$

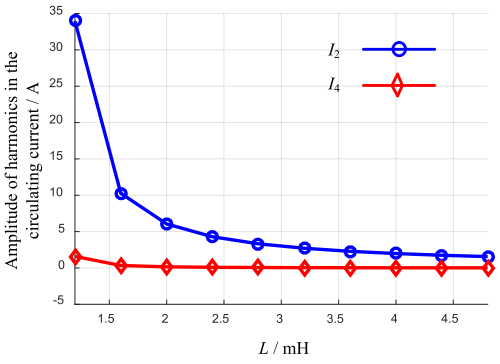

FIGURE 3. Relationship between the amplitude of harmonics in the circulating current and the effective inductance *L*.

According to the analysis above, the explicit second-order and fourth-order expressions can be obtained. Fig. 3 displays the relationship between the amplitude of harmonics in the circulating current and the effective inductance L. The point fitting curves reported here have different L, but the other parameters are kept constant (i.e., $\omega = 2\pi\cdot 50$ rad/s; $m = 0.9$; $N = 4$; $I_a = 12.16$ A; $I_{ad} = 3.72$ A; $C = 3.8\times10^{-3}$ F; sin $\varphi = 0.3424$; cos $\varphi = 0.9396$). Remarkably, the effective inductance L rises from 1.2 mH to 4.8 mH, with a substantial decline of I_2 from 33.96 A to 1.56 A. Fig. 3 also shows that the amplitude of fourth harmonic drops noticeably with increasing effective inductance L.

From Fig. 3 it can be observed that the second- and fourth-order components of harmonic are influenced by the effective inductance L.

III. ANALYSIS OF INFLUENCE OF CIS ON THE MMC SYSTEM

Compared with separated inductors, the CIs have the technical advantage of suppressing current ripple by magnetic coupling, which helps to improve power conversion efficiency and reduce the size of magnetic components. In this section, with the calculation method of the circulating current mentioned in the previous section, the influence of different CI connections on the circulating current will be discussed in detail based on the properties of the CI.

A. DEFINITION OF THE CI AND ITS INTERNAL ELECTROMAGNETIC RELATIONSHIP

In the circuit, the magnetic change caused by the current change in one coil will affect the other coil when the two coils are close enough as shown in Fig. 4(a), and such two coils as a whole is called a coupled inductor because of the internal magnetic coupling. Generally, the media to connect the magnetic flux produced by two coils is a ferromagnetic material. In real application, the structure of a CI is shown in Fig. 4(b).

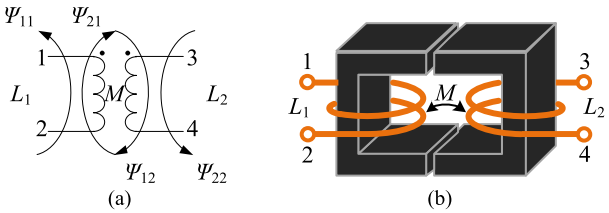

FIGURE 4. Basic structure of CI. (a) Simplified structure. (b) Application-oriented structure.

It is presented in Fig. 4 that there are four connected point in the CI belonging two coils. If current flow into one point of a coil, it will flow out from the other. L_1 and L_2 are self-inductance of coil 1 and coil 2 respectively, and M is the mutual-inductance in the two coils. The magnetic coupling degree of CIs, represented by the coefficient of mutual inductance K, is related to the coil structure, the position of coils and the magnetic medium, $K = M/(L_1L_2)^{1/2}$. Ψ_{11}, Ψ_{22} denote the magnetic flux generated by the self-inductance of inductor L_1 and inductor L_2 respectively; Ψ_{21}, Ψ_{12} denote the magnetic flux generated by the mutual-inductance; Ψ_1 and Ψ_2 denote the total magnetic flux passing through inductor L_1 and L_2 respectively. Since the magnetic flux of each coil influence that of the other core through the ferromagnetic core, the magnetic flux of each coil can be

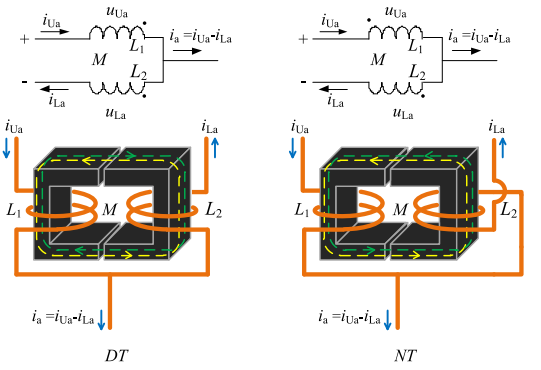

FIGURE 5. Explicit topologies as well as applied connection methods for dotted and non-dotted terminal connected CIs.

expressed by the sum of two components, as shown in (22).

$$\begin{bmatrix} \psi_1(t) \\ \psi_1(t) \end{bmatrix} = \begin{bmatrix} \psi_{11}(t) \\ \psi_{22}(t) \end{bmatrix} + \begin{bmatrix} \psi_{12}(t) \\ \psi_{21}(t) \end{bmatrix} \tag{22}$$

The directions of the self-inductance and the mutual-inductance magnetic flux may be the same or reversed, which is determined by the current directions of the coil and the winding directions of the coil. At the same time, the magnetic flux and the magnitude of current flowing through the coil have a linear relationship when the inductors are linear, hence (22) should be amended as follow

$$\begin{bmatrix} \psi_1(t) \\ \psi_2(t) \end{bmatrix} = \begin{bmatrix} L_1 & \pm M \\ \pm M & L_2 \end{bmatrix} \begin{bmatrix} i_1(t) \\ i_2(t) \end{bmatrix} \tag{23}$$

The black dots located at the top of two coils in Fig. 4 indicate the dotted terminal. When currents flow in (or flow out) one pair of terminals in the two coils at the same time, if the magnetic flux produced by self-inductance and the magnetic flux produced by mutual-inductance of the two coils have the same reference direction, the pair of terminals is considered as the dotted terminal (DT), otherwise it is non-dotted terminal (NT).

B. DECOUPLING EQUIVALENT METHOD FOR TWO-STAGE CI CONNECTIONS IN MMCS

As stated above, the unique character of the CIs determines that replacing separated inductors with CIs will have an effect on circulating currents. Generally, the PCI and NCI used in MMCs are DT and NT connections, respectively. Hereafter this text will refer to PCI with DT, and NCI is represented as NT, similarly. In most cases, the connection method of the CIs is NT connection. This part tries to expand the connection method to NT connection as well as the two-stage connection composed of DT and NT connection, and analyze them in detail. The DT and NT connection are the basis for two-stage connection, so this part starts from these two basic connections as shown in Fig. 5.

In Fig. 5, i_{Ua} represents the upper arm current, i_{La} represents the lower arm current, i_{a} represents the output current of phase a, u_{Ua} represents the voltage of CI's upper arm part and u_{La} represents the voltage of CI's lower arm part. One inductor in the CI can affect the other inductor, and this effect is represented by mutual-inductance M.

To decouple DT and NT connected CIs, the relationship between current and induced voltage should be established. In DT connected CIs, the voltage drop across each inductor can be obtained based on the magnetic flux relationship and the electromagnetic induction.

$$\begin{bmatrix} u_{\mathrm{Ua}} \\ u_{\mathrm{La}} \end{bmatrix} = \begin{bmatrix} L_1 & -M \\ -M & L_2 \end{bmatrix} \begin{bmatrix} \dfrac{d(i_{\mathrm{Ua}})}{dt} \\ \dfrac{d(i_{\mathrm{La}})}{dt} \end{bmatrix} \tag{24}$$

Equivalent transformation of (24) is

$$\begin{bmatrix} u_{\mathrm{Ua}} \\ u_{\mathrm{La}} \end{bmatrix} = \begin{bmatrix} L_1 - M & 0 & M \\ 0 & L_2 - M & -M \end{bmatrix} \begin{bmatrix} \dfrac{d(i_{\mathrm{Ua}})}{dt} \\ \dfrac{d(i_{\mathrm{La}})}{dt} \\ \dfrac{d(i_{\mathrm{a}})}{dt} \end{bmatrix} \tag{25}$$

It is clearly shown in Fig. 5 that according to the voltage relationship, the DT connected CIs can be decoupled to separated inductors. To the DT connection, the arm inductance decreases and an inductance equal to the mutual-inductance M is contributed to the load after decoupling. The inductance M mainly influences the load and the output waveform, and since this paper mainly focuses the calculation and comparison of the circulating currents, it will be ignored in the following discussion.

The expressions of the upper and lower arm inductor voltage are given in (26),

$$\begin{bmatrix} u_{\mathrm{Ua}} \\ u_{\mathrm{La}} \end{bmatrix} = \begin{bmatrix} L_1 + M & 0 & -M \\ 0 & L_2 + M & M \end{bmatrix} \begin{bmatrix} \dfrac{d(i_{\mathrm{Ua}})}{dt} \\ \dfrac{d(i_{\mathrm{La}})}{dt} \\ \dfrac{d(i_{\mathrm{a}})}{dt} \end{bmatrix} \tag{26}$$

With the analysis of the DT and NT, the two-stage connections consisting of two basic kinds of CI can be further studied. According different constitution, this paper brings forward four kinds of two-stage connections, as shown in Fig. 6.

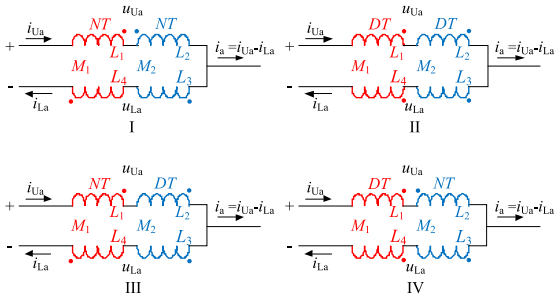

FIGURE 6. Diagram of two-stage CIs.

The application-oriented connected methods of the four groups of CIs are derived from Fig. 5. Take configuration III

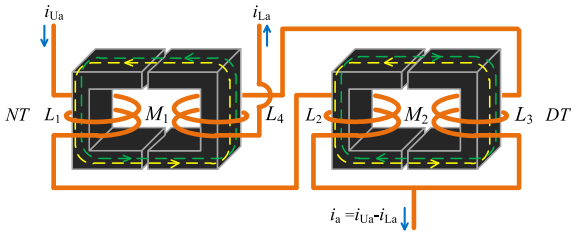

FIGURE 7. Applied connection method for the third case of two-stage CI.

as an example, the connection is shown in Fig. 7, and the theoretical discussion and the voltage relationship is expressed in (27), as shown at the bottom of this page.

According to the analysis process shown in (27), the equivalent circuit of the four kinds of two-stage connections is derived as shown in Fig. 6. The equivalent inductances are represented by L_{eq_a}, L_{eq_b}, L_{eq_c}, and L_{eq_d} respectively, and are summarized into (28).

$$L_{eq\_i} = (L_1 + L_2) + (L_3 + L_4) + 2(xM_1 + yM_2)$$
$$\begin{cases} i = a, x = 1 y = 1 \\ i = b, x = -1 y = -1 \\ i = c, x = 1 y = -1 \\ i = d, x = -1 y = 1 \end{cases} \tag{28}$$

The two-stage configuration I shown in Fig. 7 is equivalent to a NT connected CI with a large self and mutual-inductance after decoupled, and the two-stage configuration II is equivalent to a DT connected CI with a large self and mutual-inductance, which are verified by several Simulink simulations. The equivalent arm inductance obtained by the couple of two-stage configuration III and IV has the relationship shown as (28) compared with I and II configurations. By adjusting the CI coefficient of mutual inductance K, namely adjusting mutual-inductance M_1 and M_2, these two-stage connections have an influence ranging from the influence of DT connection to NT connection according to (29).

$$\begin{cases} L_{eq\_b} < L_{eq\_c} < L_{eq\_a} \\ L_{eq\_b} < L_{eq\_d} < L_{eq\_a} \end{cases} \tag{29}$$

Based on (21), the differences in equivalent arm inductance lead to the differences of circulating current. The NT connection can effectively supress the circulating current, whule the DT connection will amplify the circulating current.

TABLE 1. Simulation parameters.

Items	Values
Rated DC-link voltage	100 V
Rated line-to-line voltage at AC side	45 V
AC side frequency	50 Hz
Numbers of SMs per arm	4
DC voltage per SM	25 V
SM capacitor	3.8 mF
Self-inductance of arm inductor	L_1= L_4=1.2 mH L_2= L_3=0.3 mH
Mutual-inductance of arm inductor	M_1=1.2 mH, M_2=0.3 mH
Arm inductor resistance	0.016 Ω and 0.006 Ω
Switching frequency	2 kHz
Operating power range	from 607.5 W to 2430 W
Load resistance	5 Ω
Load inductance	0 or 5.8 mH

IV. SIMULATION RESULTS

In order to explore the effect of different kinds of connection on the circulating current, a three-phase MMC with CIs is built in the MATLAB/Simulink environment. The parameters of the model are shown in Table 1.

In order to prove the correctness of the proposed even-order harmonic expression and verify the influence of CI connections on the circulating currents, the simulation case study under various conditions is carried out.

Simulation results indicate that L_{eq_a} and L_{eq_b} are equivalent to NT and DT connection respectively, while L_{eq_c} and L_{eq_d} own a property between L_{eq_a} and L_{eq_b}. As a consequence, assessment of impacts of the total four kinds of two-stage connections on the circulating current can be implemented by performance observation of the MMC with a single equivalent DT or NT connected CI.

The simulation case study are divided into two groups, the first group keeps the apparent power of 607.5VA as a constant, and the power factor is taken as 1, and 0.94; the second group constantly keeps the power factor as 1, and the apparent power is taken as 607.5VA, and 2430VA. In the simulation case study, the control group chooses the MMC with one NT connected CI and one DT connected CI, and the simulative group selects the MMC model with the DT and NT connected CIs.

As mentioned above, the simulation case study includes three sub experiments. Fig. 8 (a), (b) shows the circulating currents of MMC with one NT connected and one DT connected, DT and NT connected CIs when apparent power is constant and the power factor is 1, and 0.94 respectively.

$$\begin{bmatrix} u_{Ua} \\ u_{La} \end{bmatrix} = \begin{bmatrix} L_1 + L_2 & M_1 - M_2 \\ -M_2 + M_1 & L_3 + L_4 \end{bmatrix} \begin{bmatrix} \frac{d(i_{Ua})}{dt} \\ \frac{d(i_{La})}{dt} \end{bmatrix}$$
$$= \begin{bmatrix} (L_1 + M_1) + (L_2 - M_2) & 0 & -M_1 + M_2 \\ 0 & (L_3 - M_2) + (L_4 + M_1) & -M_2 + M_1 \end{bmatrix} \cdot \begin{bmatrix} \frac{d(i_{Ua})}{dt} \\ \frac{d(i_{La})}{dt} \\ \frac{d(i_{La})}{dt} \end{bmatrix} \tag{27}$$

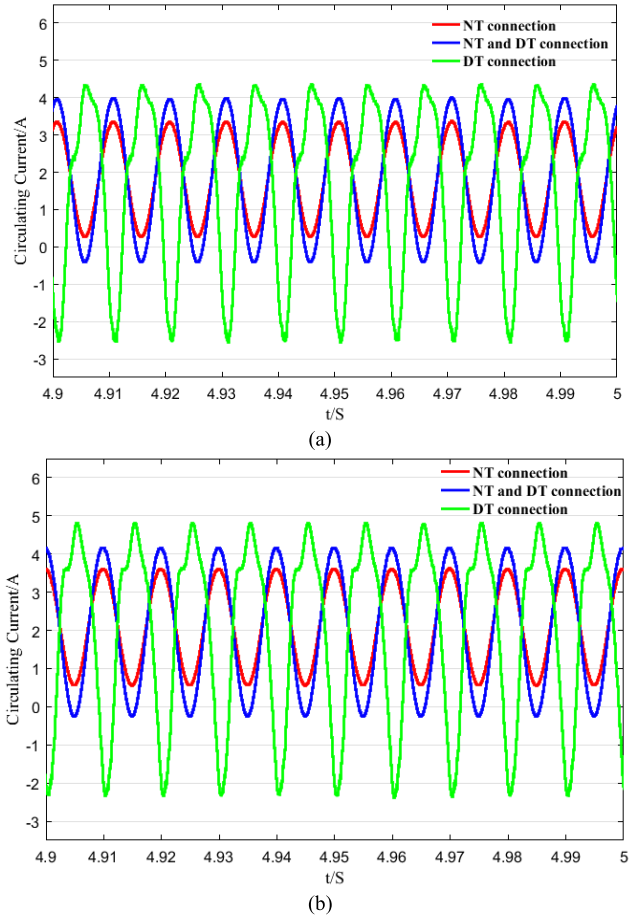

FIGURE 8. Comparison of circulating currents. (a) S = 607.5VA, PF = 1. (b) S = 607.5VA, PF = 0.94.

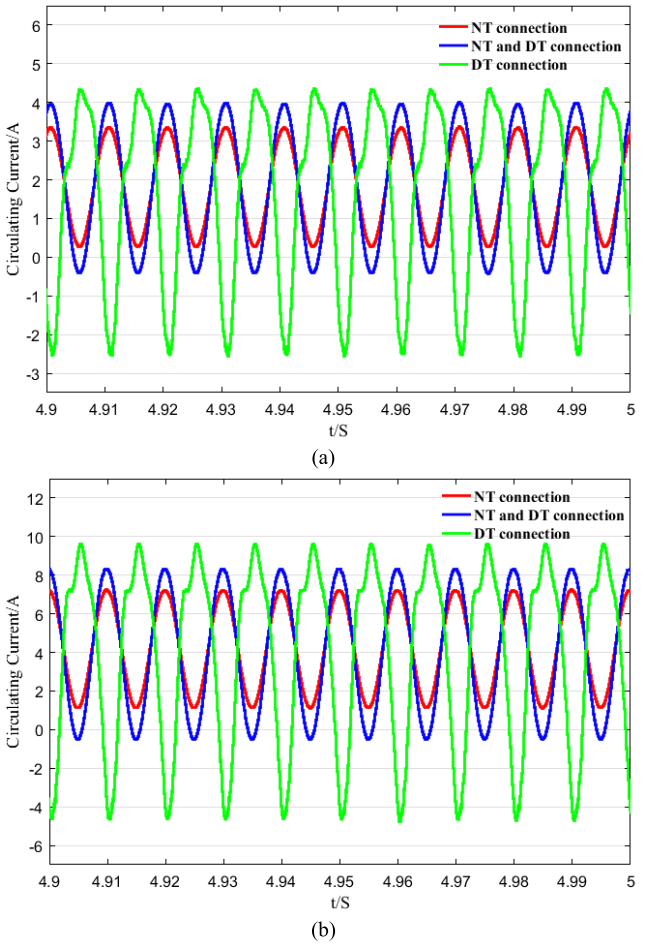

FIGURE 9. Comparison of circulating currents. (a) PF = 1, S = 607.5VA. (b) PF = 1, S = 2430VA.

Fig. 10 (a), (b) shows the circulating currents of MMC with one NT connected and one DT connected, DT and NT connected CIs when power factor is constant and apparent power is 607.5VA, 2430kVA respectively.

A qualitative conclusion is concluded from Fig. 8 and Fig. 9 that under the same conditions, the NT connected CI inhibits the circulating current, while the DT connected CI amplifies the circulating current. Furthermore, the suppression/amplification effect is very significant for second-order and fourth-order harmonic.

In order to discuss this effect more accurately, a quantitative analysis of the circulating current is needed. Under the above experiment conditions, the sole variable in the second-order harmonic expression (21) is the inductance, and the equivalent inductance of CIs obtained by decoupling equivalent method can be used to calculate the second-order harmonic of the circulating current. Take the NT connection as an example, the calculation and simulation results of second-order harmonic under different experiment conditions are shown in Fig. 10, which prove the accuracy of the second-order harmonic expression.

The comparison among the second-order harmonic of circulating currents in MMC with DT and NT connected

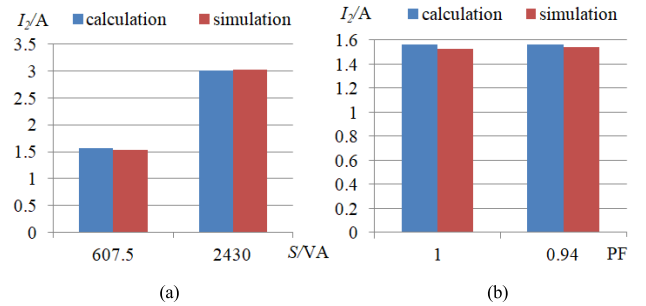

FIGURE 10. Calculation and simulation results of second-order harmonic. (a) PF = 1, S = 607.5VA and 2430VA. (b) S = 607.5VA, PF = 1, and 0.94.

inductors, DT connected inductors and NT connected inductors under different conditions are shown in Fig. 11.

According to the expression (21), both equivalent inductance and the magnitude of second-order harmonic affect the magnitude of fourth-order harmonic. The first step is to prove the accuracy of the fourth-order harmonic expression derived in this paper, as shown in Fig. 12.

The comparison among the fourth-order harmonic of circulating currents is shown in Fig. 13.

With the illustrations from Fig. 10 to Fig. 13, the accuracy of the expressions for the second-order and

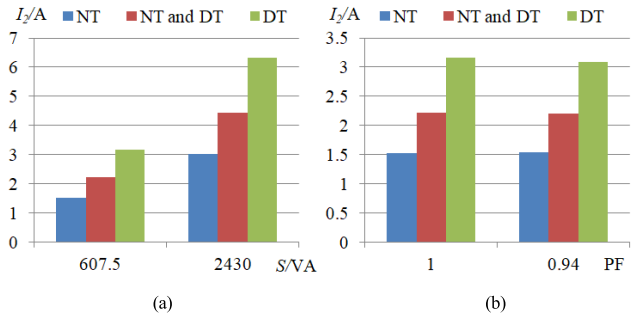

FIGURE 11. Simulation results of second-order harmonic. (a) PF = 1, S = 607.5VA, and 2430VA. (b) S = 607.5VA, PF = 1, and 0.94.

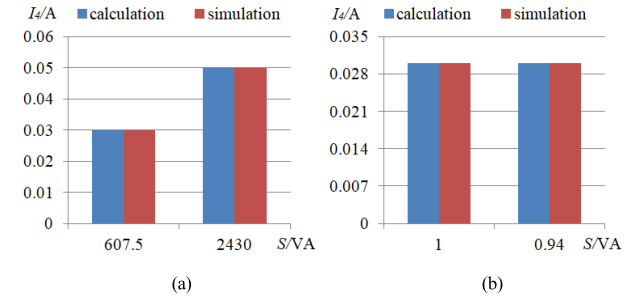

FIGURE 12. Calculation and simulation results of fourth-order harmonic. (a) PF = 1, S = 607.5VA and 2430VA. (b) S = 607.5VA, PF = 1, and 0.94.

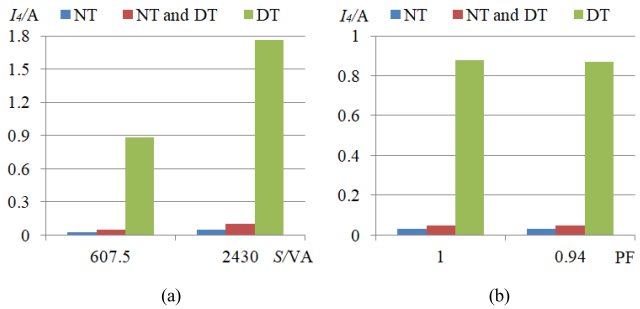

FIGURE 13. Simulation results of fourth-order harmonic. (a) PF = 1, S = 607.5VA, and 2430VA. (b) S = 607.5VA, PF = 1, and 0.94.

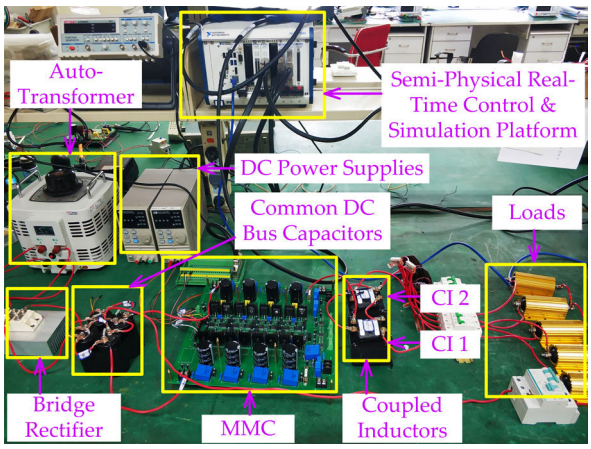

FIGURE 14. Experiment prototype of the MMC system.

fourth-order harmonic in the circulating current and the effectiveness of the decoupling equivalent method for CIs are verified.

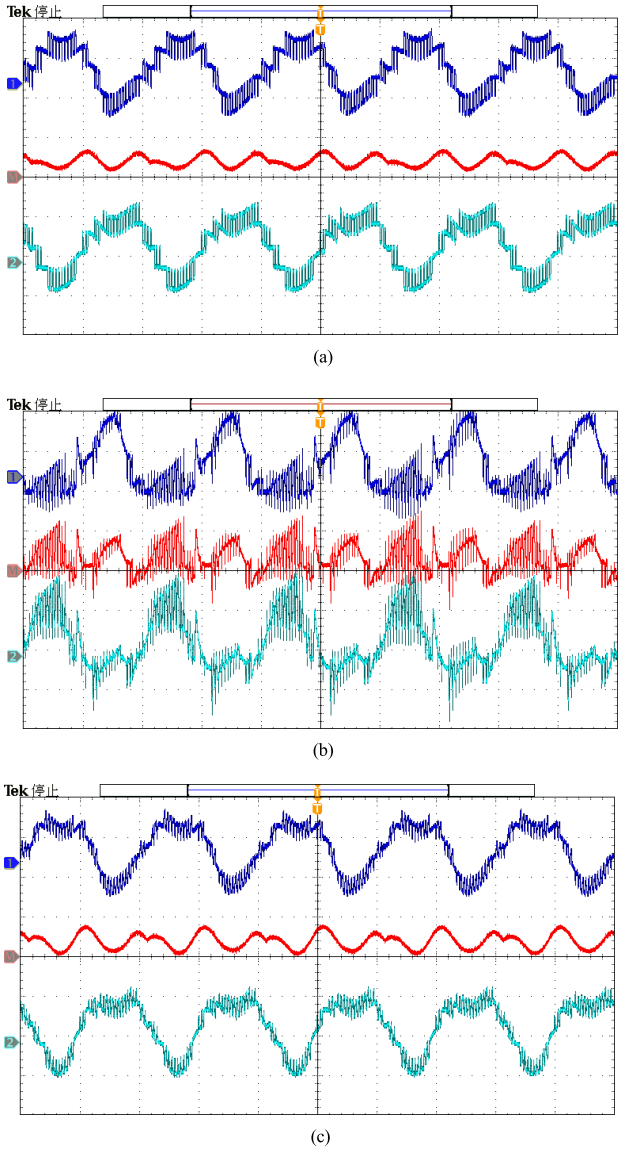

FIGURE 15. Experimental results of the arm currents and circulating current with the load of 5 Ω. (a) CI configuration I (Ch1: 5 A/div, Ch2: 5 A/div, and ChM: 5 A/div). (b) CI configuration II (Ch1: 5 A/div, Ch2: 5 A/div, and ChM: 5 A/div). (c) CI configuration III (Ch1: 5 A/div, Ch2: 5 A/div, and ChM: 5 A/div).

Based on the previous discussion, it is qualitatively and quantitatively proved that a NT terminal connected CI can significantly reduce the circulating current harmonic, and the higher the order of the circulating current harmonic, the larger the suppression is. A DT connected CI can significantly amplify the circulating current harmonic, and the higher the order of the circulating current harmonic, the larger the amplification is. For the MMC containing a two-stage CI, the influence ranges from suppression to amplification as its equivalent inductance is between that of DT and NT connected CIs.

V. EXPERIMENTAL VERIFICATION

In order to verify the correctness of theoretical analysis above and the effectiveness of two-stage CIs on the circulating

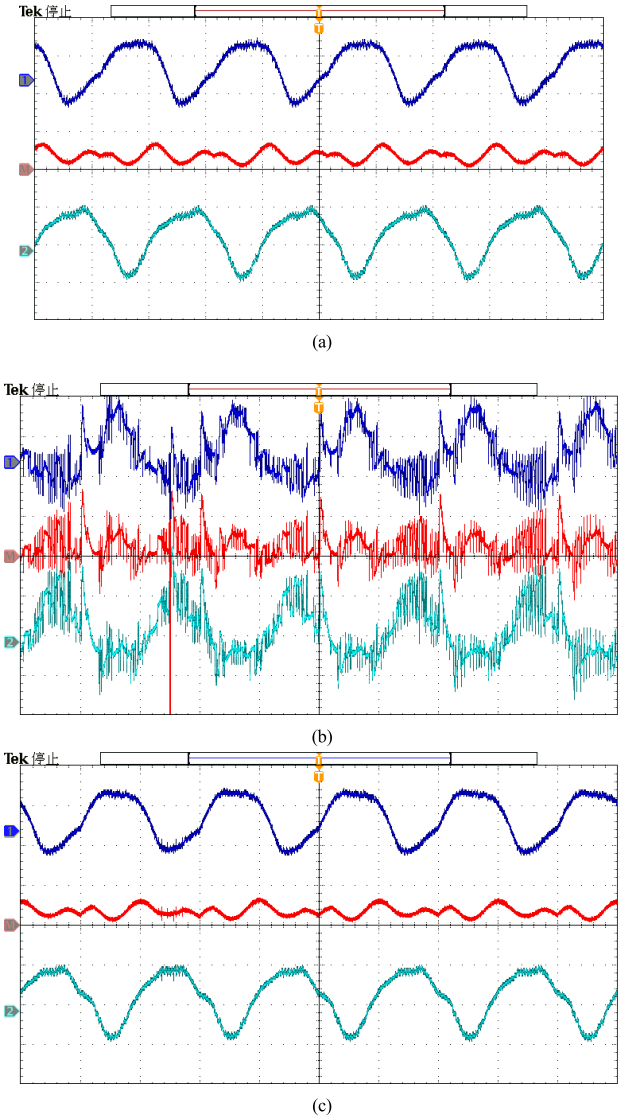

FIGURE 16. Experimental results of the arm currents and circulating current with the load of 5 Ω and 5.8 mH. (a) CI configuration I (Ch1: 5 A/div, Ch2: 5 A/div, and ChM: 5 A/div). (b) CI configuration II (Ch1: 5 A/div, Ch2: 5 A/div, and ChM: 5 A/div). (c) CI configuration III (Ch1: 5 A/div, Ch2: 5 A/div, and ChM: 5 A/div).

current, a three-phase 5-level MMC low-voltage prototype is built using a semi-physical real-time control system, which performs sampling and control algorithms, and outputs PWM signals. The Experiment prototype of the MMC system is shown in Fig. 14.

For the prototype construction, two kinds of CIs (CI 1: Bel Signal Transformer CL-12-24, and CI 2: Bel Signal Transformer CL-25-50) with self-inductance of 1.2 mH and 0.3 mH are included, which have the coefficient of mutual inductance $K = 1$. The three-phase two-stage coupled inductors contain a total of 6 CIs with EI core configuration, using silicon steel sheets as magnetic core materials.

In the MMC system, the switching frequency is 2 kHz. The output of the single-phase uncontrollable full-bridge rectifier is parallel connected to the common DC bus capacitor bank, which provides a stable bus voltage for the MMC. The system parameters used for the experiments are the same as Table 1.

In the experimental verification, the two-stage CI configuration I, II, and III (see Fig. 6) have been tested to verify the influence of CIs on the circulating current. Two kinds of loads, which are the resistive load of 5 Ω and the resistance-inductance load of 5 Ω plus 5.8 mH, are adopted in the experiments.

The experimental results of the arm currents and circulating current are shown in Fig. 15 and 16.

At first, the comparison of circulating currents with the load of 5 Ω is demonstrated in Fig. 15. As it can be seen in this figure, he DT connection method amplifies the circulating current, the NT connection method suppresses it, and the series connection of DT and NT CIs has an effect between NT and DT connection when the load is a resistive load.

In a similar way, Fig. 16 illustrates the comparison of circulating currents with the load of 5 Ω and 5.8 mH. It is observed from Fig. 16 that when the load consists of resistor and inductor, the two-stage CI configurations have the same influence on circulating current with that when the load is a resistor.

As expected, the NT connected CIs could suppress the circulating current, while the DT connected CIs could amplify the circulating current. The figures illustrate that the results are consistent with the simulation results in Fig. 8 and Fig. 9.

VI. CONCLUSION

In this work, detailed topology derivation of the CIs used in MMC based HVDC systems is brought forward firstly. A family of CI topologies is derived with different two-stage connections and different coupling configurations, including DT and NT connections. In addition to the topology derivation, the influence of the two-stage CIs on circulating currents of the MMC is also discussed by employing the accurate circulating current estimation and decoupling equivalent method. In order to obtain a comprehensive insight of the proposed CI topologies, the simulation and experimental case studies for the MMC with CIs are carried out. Through the theoretical analysis and case studies, the conclusion can be drawn that the NT connection suppresses the circulating current, DT connection amplifies the circulating current, and the effect of two-stage connection is between suppression and amplification.

REFERENCES

[1] N. Flourentzou, V. G. Agelidis, and G. D. Demetriades, "VSC-based HVDC power transmission systems: An overview," *IEEE Trans. Power Electron.*, vol. 24, no. 3, pp. 592–602, Mar. 2009.

[2] V. G. Agelidis, G. D. Demetriades, and N. Flourentzou, "Recent advances in high-voltage direct-current power transmission systems," in *Proc. IEEE Int. Conf. Ind. Technol.*, Mumbai, India, Dec. 2006, pp. 206–213.

[3] M. M. Alharbi and M. L. Crow, "Modeling of multi-terminal VSC-based HVDC system," in *Proc. IEEE Power Energy Soc. Gen. Meeting (PESGM)*, Boston, MA, USA, Jul. 2016, pp. 1–5.

[4] Y. Liu and Z. Chen, "A flexible power control method of VSC-HVDC link for the enhancement of effective short-circuit ratio in a hybrid multi-infeed HVDC system," *IEEE Trans. Power Syst.*, vol. 28, no. 2, pp. 1568–1581, May 2013.

[5] J. Burr, S. Finney, and C. Booth, "Comparison of different technologies for improving commutation failure immunity index for LCC HVDC in weak AC systems," in *Proc. 11th IET Int. Conf. AC DC Power Transmiss.*, Birmingham, U.K., Feb. 2015, pp. 1–7.
[6] J. W. Feltes, B. D. Gemmell, and D. Retzmann, "From smart grid to super grid: Solutions with HVDC and FACTS for grid access of renewable energy sources," in *Proc. IEEE Power Energy Soc. Gen. Meeting*, Detroit, MI, USA, Jul. 2011, pp. 1–6.
[7] Y. Xue, X.-P. Zhang, and C. Yang, "Commutation failure elimination of LCC HVDC systems using thyristor-based controllable capacitors," *IEEE Trans. Power Del.*, vol. 33, no. 3, pp. 1448–1458, Jun. 2018.
[8] S. P. Teeuwsen, "Modeling the Trans bay cable project as voltage-Sourced converter with modular multilevel converter design," in *Proc. IEEE Power Energy Soc. Gen. Meeting*, Detroit, MI, USA, Jul. 2011, pp. 1–8.
[9] W. Zhibing, X. Yang, and W. Xitian, "Coordinated control strategy of reactive power for large-scale wind power transmission by LCC-HVDC links," *J. Eng.*, vol. 2017, no. 13, pp. 1082–1086, 2017.
[10] N. A. Belda, C. A. Plet, and R. P. P. Smeets, "Analysis of faults in multiterminal HVDC grid for definition of test requirements of HVDC circuit breakers," *IEEE Trans. Power Del.*, vol. 33, no. 1, pp. 403–411, Feb. 2018.
[11] J. Xu, C. Zhao, Y. Xiong, C. Li, Y. Ji, and T. An, "Optimal design of MMC levels for electromagnetic transient studies of MMC-HVDC," *IEEE Trans. Power Del.*, vol. 31, no. 4, pp. 1663–1672, Aug. 2016.
[12] P. Bresesti, W. L. Kling, R. L. Hendriks, and R. Vailati, "HVDC connection of offshore wind farms to the transmission system," *IEEE Trans. Energy Convers.*, vol. 22, no. 1, pp. 37–43, Mar. 2007.
[13] S. Debnath, J. Qin, B. Bahrani, M. Saeedifard, and P. Barbosa, "Operation, control, and applications of the modular multilevel converter: A review," *IEEE Trans. Power Electron.*, vol. 30, no. 1, pp. 37–53, Jan. 2015.
[14] D. Jovcic and A. A. Jamshidifar, "Phasor model of modular multilevel converter with circulating current suppression control," *IEEE Trans. Power Del.*, vol. 30, no. 4, pp. 1889–1897, Aug. 2015.
[15] H. Yang and M. Saeedifard, "A capacitor voltage balancing strategy with minimized AC circulating current for the DC-DC modular multilevel converter," *IEEE Trans. Ind. Electron.*, vol. 64, no. 2, pp. 956–965, Feb. 2017.
[16] S. Allebrod, R. Hamerski, and R. Marquardt, "New transformerless, scalable modular multilevel converters for HVDC-transmission," in *Proc. IEEE Power Electron. Spec. Conf.*, Rhodes, Greece, Jun. 2008, pp. 174–179.
[17] M. Hagiwara and H. Akagi, "Control and experiment of pulsewidth-modulated modular multilevel converters," *IEEE Trans. Power Electron.*, vol. 24, no. 7, pp. 1737–1746, Jul. 2019.
[18] M. Saeedifard and R. Iravani, "Dynamic performance of a modular multilevel back-to-back HVDC system," *IEEE Trans. Power Del.*, vol. 25, no. 4, pp. 2903–2912, Oct. 2010.
[19] K. Wang, Y. Li, Z. Zheng, and L. Xu, "Voltage balancing and fluctuation-suppression methods of floating capacitors in a new modular multilevel converter," *IEEE Trans. Ind. Electron.*, vol. 60, no. 5, pp. 1943–1954, May 2013.
[20] X. Yang, J. Li, X. Wang, W. Fan, and T. Q. Zheng, "Circulating current model of modular multilevel converter," in *Proc. Asia–Pacific Power Energy Eng. Conf.*, Wuhan, China, Mar. 2011, pp. 1–6.
[21] K. Ilves, S. Norrga, L. Harnefors, and H.-P. Nee, "Analysis of arm current harmonics in modular multilevel converters with main-circuit filters," in *Proc. Int. Multi-Conf. Syst. Signals Devices*, Chemnitz, Germany, Mar. 2012, pp. 1–6.
[22] M. Vasiladiotis, N. Cherix, and A. Rufer, "Accurate capacitor voltage ripple estimation and current control considerations for grid-connected modular multilevel converters," *IEEE Trans. Power Electron.*, vol. 29, no. 9, pp. 4568–4579, Sep. 2014.
[23] K. Ilves, A. Antonopoulos, S. Norrga, and H.-P. Nee, "Steady-state analysis of interaction between harmonic components of arm and line quantities of modular multilevel converters," *IEEE Trans. Power Electron.*, vol. 27, no. 1, pp. 57–68, Jan. 2012.
[24] Q. Song, W. Liu, X. Li, H. Rao, S. Xu, and L. Li, "A steady-state analysis method for a modular multilevel converter," *IEEE Trans. Power Electron.*, vol. 28, no. 8, pp. 3702–3713, Aug. 2013.
[25] S. Rohner, S. Bernet, M. Hiller, and R. Sommer, "Modelling, simulation and analysis of a modular multilevel converter for medium voltage applications," in *Proc. IEEE Int. Conf. Ind. Technol.*, Vina del Mar, Chile, Mar. 2010, pp. 775–782.
[26] X. Li, B. Zhang, D. Qiu, L. Qu, G. Zhang, and F. Xie, "Modular multilevel converters using split wound coupled inductors," in *Proc. 41st Annu. Conf. IEEE Ind. Electron. Soc.*, Yokohama, Japan, Nov. 2015, pp. 002713–002716.
[27] X. Li, L. Qu, B. Zhang, H. Liao, and Z. Zhang, "A novel topolgoy of multi-level converters using split wound coupled inductors," in *Proc. 43rd Annu. Conf. IEEE Ind. Electron. Soc.*, Beijing, China, Oct./Nov. 2017, pp. 4834–4838.
[28] J. Kucka, D. Karwatzki, L. Baruschka, and A. Mertens, "Modular multilevel converter with magnetically coupled branch inductors," *IEEE Trans. Power Electron.*, vol. 32, no. 9, pp. 6767–6777, Sep. 2017.
[29] J. Kucka, D. Karwatzki, L. Baruschka, and A. Mertens, "Improved modular multilevel converter topology with magnetically coupled branch inductors," in *Proc. IEEE Energy Convers. Congr. Expo. (ECCE)*, Montreal, QC, Canada, Sep. 2015, pp. 3593–3600.
[30] W. Kawamura, M. Hagiwara, and H. Akagi, "Design and evaluation of AC inductors indispensable to a modular multilevel cascade converter (MMCC-TSBC) for medium-voltage motor drives," in *Proc. IEEE 2nd Int. Future Energy Electron. Conf. (IFEEC)*, Taipei, Taiwan, Nov. 2015, pp. 1–6.
[31] W. Kawamura, M. Hagiwara, H. Akagi, M. Tsukakoshi, R. Nakamura, and S. Kodama, "AC-inductors design for a modular multilevel TSBC converter, and performance of a low-speed high-torque motor drive using the converter," *IEEE Trans. Ind. Appl.*, vol. 53, no. 5, pp. 4718–4729, Sep./Oct. 2017.
[32] H. Nademi, L. Norum, and A. Das, "A new circuit of modular multilevel inverter for grid-connected photovoltaic conversion plants," in *Proc. IEEE 42nd Photovoltaic Spec. Conf. (PVSC)*, New Orleans, LA, USA, Dec. 2015, pp. 1–6.
[33] B. Džonlaga, D. R. Joca, L. Quéval, and J. C. Vannier, "Transient analysis of a modular multilevel converter with coupled arm inductors," in *Proc. IEEE Appl. Power Electron. Conf. Expo. (APEC)*, San Antonio, TX, USA, Mar. 2018, pp. 1662–1667.

KE SHEN (S'10–M'15) received the B.S., M.S., and Ph.D. degrees in electrical engineering from the Harbin Institute of Technology, Harbin, China, in 2007, 2009, and 2014, respectively.

From 2011 to 2012, he was a Visiting Ph.D. Student with the Center for Ultra-Wide-Area Resilient Electric Energy Transmission Networks, The University of Tennessee, Knoxville, TN, USA, where he was supported by the Chinese Scholarship Council. Since 2014, he has been with the School of Automation, Northwestern Polytechnical University, Xi'an, China, where he is currently an Assistant Professor. He is also a Senior Research Engineer with the Shaanxi Key Laboratory of Small and Special Electrical Machine and Drive Technology, Xi'an. His current research interests include power electronics for more electric aircrafts, multilevel converters, and energy conversion.

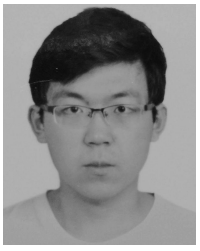

SHAOZHE WANG (S'17) received the B.S. degree in electrical engineering from the Northwestern Polytechnical University, Xi'an, China, in 2019. He is currently pursuing the M.S. degree in electrical engineering with Texas A&M University, College Station, TX, USA.

His research interests include multilevel converters, renewable energy conversion, and electric vehicle.

DAN ZHAO (S'17) received the B.S. degree in electrical engineering from the Hebei University of Technology, Tianjin, China, in 2009, and the M.S. degree in electrical engineering from the Harbin Institute of Technology, Harbin, China, in 2011. She is currently pursuing the Ph.D. degree in electrical engineering with Northwestern Polytechnical University, Xi'an, China.

From 2011 to 2014, she was with Monolithic Power System, Inc., Hangzhou, China. From 2014 to 2017, she was with Aviation Industry Corporation, Xi'an. Her research interests include power electronics for more electric aircraft, motor drive systems, and electromagnetic compatibility.

GUODONG ZHAO (S'18) received the B.S. degree in electrical engineering from the Shenyang University of Technology, Shenyang, China, in 2017. He is currently pursuing the M.S. degree in electrical engineering with Northwestern Polytechnical University, Xi'an, China.

His research interests include multilevel converters, motor driver systems and modeling, and control algorithms.